Compensation of the Thermal Effect in a Mounted Microbubble Resonator

Zheng-Yu Wang, Hong-Liang Ren, Hong-Yi Qiao, Rui Niu, Guang-Can Guo, and Chun-Hua Dong

***Abstract*—To mitigate the temperature dependence of the resonance frequency in microcavities, athermal photonic devices have been developed by incorporating materials with an opposite thermo-optical coefficient (TOC). Here, we conduct an experimental demonstration of the athermal effect in a microbubble resonator, employing an aluminum (Al) holder for its mounting. By converting the thermal expansion of the holder into controlled geometry adjustments in the microbubble resonator, we achieve athermal optical modes at a specific temperature. The athermal compensation is accomplished by counterbalancing the pulling force resulting from the thermal expansion of the Al holder against the thermal characteristics of the material, specifically SiO_2. Especially, the optical modes located around the equator are particularly susceptible to the influence of the pulling force exerted by the Al holder. This temperature-insensitive feature of the resonance establishes a new avenue towards athermal microresonator through this special structure.**

***Index Terms*—Whispering gallery mode, thermal effect, athermal microresonator.**

I. Introduction

OVER the past few decades, whispering gallery mode (WGM) resonators have garnered significant attention across various research domains, such as cavity quantum electrodynamics, ultra-low-threshold lasers, cavity optomechanics, frequency comb, modulator and ultrasensitive sensing [1], [2], [3], [4], [5], [6], [7], [8], [9], [10], [11], [12], due to their high quality (Q) factors and relatively small mode volumes [13], [14]. The circulating optical field in a WGM microcavity can significantly improve photon-matter interaction, resulting in strong microcavity heating due to optical absorption [15], [16], [17]. For the heated microcavity, the resonance frequency may deviate far away from its initial frequency due to thermo-refractive and thermal-expansion effects [15]. A number of thermal phenomena have led to the mode drift, such as thermal broadening and suppression [15], [18], [19], [20], thermal oscillation [21], [22], [23], [24], [25], [26], [27] and thermal noise [28], [29]. Although thermal effect could lock the laser detuning to the mode frequency and thermally tune the free spectral range (FSR), it would induce thermal noise and instability in the microresonator. To mitigate undesired thermal effect, researchers often explore a combination of different materials with opposite temperature coefficients (TOC), a configuration commonly referred to as an athermal hybrid microresonator [30], [31], [32], [33], [34], [35], [36]. Nevertheless, achieving the athermal effect often comes at the cost of compromising the Q factor, which drops below 10^6 due to either material absorption or the immaturity of fabrication techniques for diverse materials, such as the TiO_2 [37], Ta_2O_5 [35] and organic materials (PDMS [21] or PMMA [23]). Additionally, the interplay of opposing thermo-optic effects can result in thermal oscillations within the hybrid microresonator. Consequently, an alternative approach is required to mitigate the thermal effect while maintaining both a high Q factor and stability simultaneously.

An innovative effort to counteract long-term frequency drift and thermodynamic noise is observed in magnesium fluoride (MgF_2) microcavity [38], which exhibits a thermal expansion 15 times greater than its thermo-refractive effect. To counterbalance for the significant thermal expansion, the resonator is enclosed between layers of a nearly zero or slightly negative expansion material (e.g. Zerodur). However, it is in principle impossible to completely eliminate thermal frequency drift, even while maintaining a high Q factor. When a highly mechanically tunable system is available, the powerful negative expansion effect can be employed to counteract the positive thermo-refractive effect effectively. The tunable optical microbubble resonator, featuring a hollow center, has successfully demonstrated the effective utilization of a negative expansion effect [39]. The optical mode is blue drifted about 5.5 nm by stretching two poles of the microbubble fixed on the piezoelectric transducer (PZT) stage which undergoes about 30 μm displacement. Consequently, we can developed a mechanically tunable microbubble resonator with effective negative thermal expansion in a specific design to realize an athermal microcavity.

In this paper, we present a novel approach to constructing an athermal microresonator. This involves a meticulous balance between the positive TOC and a naturally occurring negative effect caused by the material's thermal expansion during cavity mounting on the aluminum (Al) holder. In comparison to

Manuscript received 20 November 2023; revised 19 December 2023; accepted 20 December 2023. Date of publication 25 December 2023; date of current version 10 January 2024. This work was supported in part by the National Natural Science Foundation of China under Grants 12293052, 11934012, 12104442, 92050109, 92250302, and 12304435, and in part by the Fundamental Research Funds for the Central Universities, the China Postdoctoral Science Foundation under Grant 2023M733414. *(Corresponding authors: Hong-Liang Ren; Chun-Hua Dong.)*

Zheng-Yu Wang, Hong-Yi Qiao, Rui Niu, Guang-Can Guo, and Chun-Hua Dong are with the CAS Key Laboratory of Quantum Information, University of Science and Technology of China, Hefei 230026, China, and also with the CAS Center For Excellence in Quantum Information and Quantum Physics, University of Science and Technology of China, Hefei 230026, China (e-mail: chunhua@ustc.edu.cn).

Hong-Liang Ren is with the College of Information Engineering, Zhejiang University of Technology, Hangzhou 310023, China (e-mail: hlren@zjut.edu.cn).

Digital Object Identifier 10.1109/JPHOT.2023.3346475

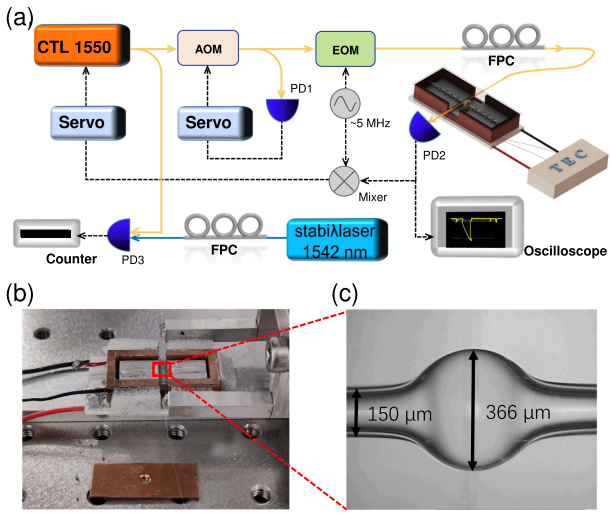

Fig. 1. (a) Schematic of the bubble microcavity characterization. The wavelength continuously tunable laser is either scanned or locked around 1542 nm to refer with the stabi λ laser 1542 nm. AOM: Acousto-optic modulator; EOM: Electro-optic modulator; TEC: thermoelectric cooler; FPC: fiber polarization controller; PD: photodetector. (b) Al holder for mounting the bubble resonator. (c) Typical microscopy of the microbubble resonator.

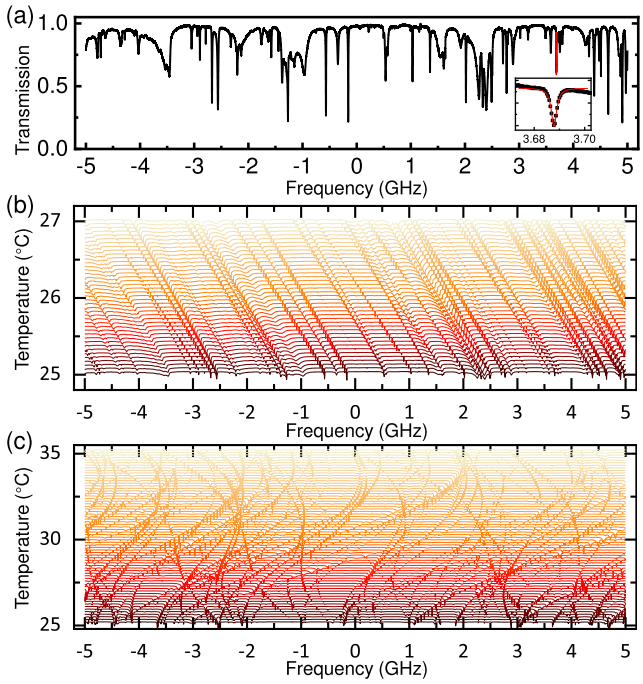

Fig. 2. Resonance frequency shift of the WGM as a function of operating temperature. (a) Free-standing bubble resonator transmission spectrum at 25°C. The inset is the transmission of the corresponding optical mode with a Lorentzian fitting (red line). (b) Free-standing bubble resonator transmission spectra show that these resonances shift to red side with the temperature linearly. (c) Transmission spectra of the mounted microbubble resonator reveal that initially, these resonances shift to the blue side. However, as the temperature reaches approximately 35 °C, these resonances gradually shift towards the red side, signifying the temperature quiet point (TQP).

fabricating the hybrid material with opposite TOC, the mounted microbubble resonator offers a more straightforward preparation process and achieves a higher Q factor about 2×10^7. In our experiment, we fabricate the microbubble resonator using the capillary tube, measure its transmission spectrum and trace the resonance mode around 1542 nm. Firstly, we compare two fixed modes, i.e., fixing only one pole and two poles of the capillary tube. Then we investigate the impact of the fiber taper coupling location and the fixation status of the ultraviolet glue. Finally, we lock the laser frequency onto the selected resonance to confirm the athermal microresonator, and the results agree well with the design expectations.

II. Experimental Setup and Results

Fig. 1 shows the experimental setup of an athermal microresonator. A tunable laser (CTL 1550) is coupled into the microbubble resonator using a fiber taper, which is securely attached to the resonator to maintain a stable coupling state. The fiber polarization controllers (FPCs) are used to control the polarization of input lasers. A reference laser operating around 1542 nm (stabi λ laser 1542, 194.369489384(5) THz) is utilized for accurate monitoring of the resonant frequency shift in the microcavity. During the experiment, the power of light is stabilized by the acousto-optic modulator (AOM). The microbubble resonator is mounted on an Al holder. The poles of the capillary tube are securely fixed using ultraviolet glue, as depicted in Fig. 1(b). The Al holder is enclosed within a copper (Cu) box to minimize environmental influences, such as air turbulence. The temperature inside the Cu box is monitored using a thermistor and regulated by a semiconductor cooler, controlled by the thermoelectric cooler (TEC). Subsequently, the photodetector (PD) is utilized to detect the transmission spectrum, which is then recorded using an oscilloscope (OSC).

The microbubble resonator is fabricated using an internally pressurized glass capillary tube (Polymicro Flexible Fused Silica Capillary Tubing, TSP075150), which is locally melt by the arc from the optical fiber fusion splicer [40], [41], [42], [43]. Initially, one end of a silica capillary is fused and sealed using a fiber fusion splicer. Using a syringe, air is concurrently injected into the capillary tube, which is precisely repositioned between the two discharge electrodes of the splicer. Finally, the segment of the capillary heated by the discharge gradually expands, forming a bubble under the pressure of the introduced gas. By repeatedly heating and inflating, we can achieve a microbubble of the desired size. The typical diameter of the micro-bubble is approximately 366 μm, while the capillary tube has an outer diameter of 150 μm and an inner diameter of 75 μm, as shown in Fig. 1(c).

First of all, we have studied the optical modes in the microbubble. A typical transmission spectrum of the WGM mode is shown in Fig. 2(a). A series of optical modes are obtained when the wavelength is scanned with the range of around 10 GHz. The Q factor of optical modes could be observed as high as 7.8×10^7, as shown in the inset of Fig. 2(a). As the temperature increases, the positive thermo-refractive and thermal expansion effects of silica microbubble may cause a red shift in the resonance frequency [15], [44]. Fig. 2(b) shows the red resonances shift in a free-standing bubble resonator when the temperature is slowly increased from 25 °C to 27 °C with the step size of

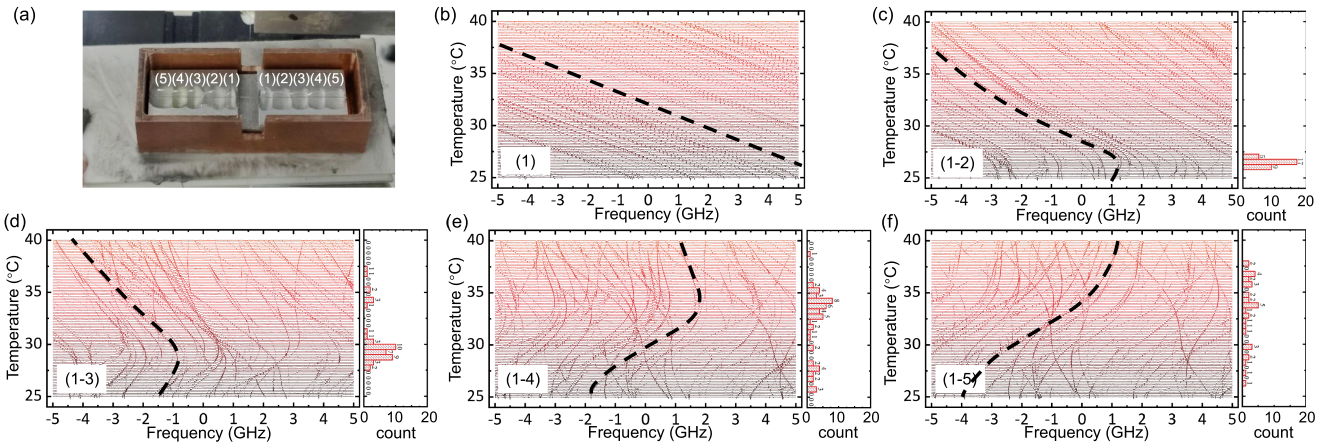

Fig. 3. Stretching the capillary tube symmetrically with multiple increasing fixed points by ultraviolet glue from the inner position to the outer position. (a) Picture of mounted microresonator with the symmetrical of fixed points, numbered from (1) to (5). (b)–(f) Transmission spectra versus temperature of the mounted microbubble resonator are separately presented for the cases of adding fixed positions (1), (1–2), (1–3), (1–4), and (1–5). Obviously, the TQP progressively shifts towards the higher temperature range from (b) to (f), indicating the upper limit of the stretch force is improved by the increasing fixed points. Inset in (c)–(f): The histogram depicting the distribution of the TQP for all WGMs within the specified frequency range for corresponding positions.

$0.05\ ^{\circ}\mathrm{C}$. Following each temperature alteration, the system undergoes a 2-minute waiting period to stabilize before collecting the transmission spectrum. The sensitivity curve exhibits an excellent linearity in the range of temperature change, with a slope of $6.4\ \mathrm{pm}/^{\circ}\mathrm{C}$. The experimental result agrees well with the predicted theoretical value according to the TOC of the SiO_2 ($\sim 1 \times 10^{-5}/\mathrm{K}$ [45]).

Conversely, when both ends of the capillary tube are mounted on the Al holder, the resonance frequency shift of the WGM undergoes changes. The thermal expansion of the Al holder would exert a force on the capillary tube along the central axis. This action leads to the contraction of the microbubble, causing it to revert to its smaller size and inducing a blue shift in the resonance frequency, as shown in Fig. 2(c). The observation initially shows a blue shift in resonance at lower temperatures. This shift gradually transitions towards temperature insensitivity as the temperature approaches around $35\ ^{\circ}\mathrm{C}$. This point can be identified as the temperature quiet point (TQP). Following the temperature quiet point, there is a subsequent red shift in the resonance frequency. Hence, initially, the expansion of the Al holder is dominated at the beginning, exerting a force that causes the microbubble resonator to contract, leading to a reduction in radius. This contraction corresponds to the blue shift observed in the resonance. Nonetheless, the pulling force exerted by the Al holder encounters limitations as the microbubble resonator exhibits resistance. Upon achieving balance in compensation, the resonance frequency remains unchanged at the TQP, as shown in Fig. 2(c). Subsequently, the ascendancy of positive thermal characteristics takes center stage, resulting in the red ward shift of the resonance frequency. Furthermore, the microbubble resonator offers numerous optical mode families, each occupying distinct regions within the microresonator. These mode families respond variably to the pulling force exerted by the Al holder. Consequently, when the temperature undergoes changes, this discrepancy in response across modes leads to diverse frequency shifts. Hence, achieving equilibrium points across a wide range becomes readily attainable. The features of the TQP would be characterized in the following experiment.

To study the expansion force in the hybrid system, we add symmetrically and gradually multiple fixed points to two ends of the capillary tube, as indicated in Fig. 3(a). Figs. 3(b)–(f) show the transmission spectra of the mounted microbubble resonator, which is presented for the cases of adding symmetrically fixed positions (1), (1–2), (1–3), (1–4), and (1–5) on the both side of the microbubble. Within each spectrum, for the sake of generality, a tracking mode is selected as a representative example from every mode family, as indicated the black dashed lines in Figs. 3(b)–(f). The resonances exhibit a linear red shift with temperature when only the capillary tube is fixed at position (1), which has the small glue on both sides of the microbubble. In this scenario, the expansion of the Al holder have no enough adhering force to stretch the microbubble and induce the frequency blue shift. When the glue points are added symmetrically from the inside to the outside, the stretching force is more and more obvious, as show in Figs. 3(c)–(f). The transmission spectra of the mounted microbubble resonator show that the TQP progressively shifts towards the higher temperature side with increasing fixed points, which enhance the upper limit of the pulling force. In Figs. 3(c)–(f), the average TQPs are around $26.4\ ^{\circ}\mathrm{C}$, $30.3\ ^{\circ}\mathrm{C}$, $32.0\ ^{\circ}\mathrm{C}$ and $33.3\ ^{\circ}\mathrm{C}$, respectively. These results serve to provide a more intuitive validation of the conclusion drawn from the observations presented in Fig. 3. Additionally, the measured transmission reveals that each mode family exhibits a distinct temperature response, as indicated by the varying slopes of the resonance shift. Considering the diverse temperature responses, it is feasible to adjust the resonance interval solely through temperature variations within a single microcavity. Moreover, when the number of fixed points is enough, the resonance shift is becoming less sensitive to temperature changes near the TQP. As shown in Figs. 3(c)–(f), as the TQP increases, the resonance shift at the TQP gradually becomes less responsive to temperature fluctuations. We believe that enhancing the stability of the

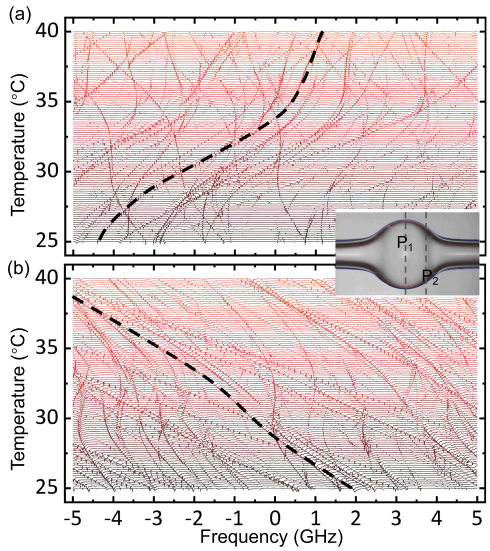

Fig. 4. (a)–(b) Typical transmission spectra versus temperature of the mounted microbubble resonator with different coupling positions P1 and P2, respectively. Inset: The microscopy of the microbubble resonator with the fiber taper coupling positions of P1 or P2.

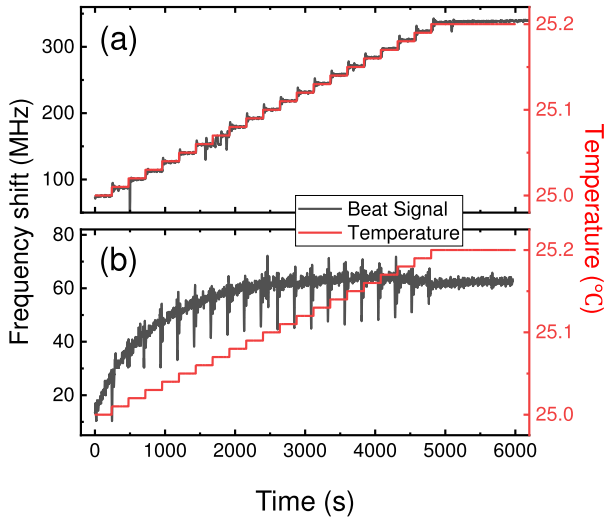

Fig. 5. (a) When locking a CTL to a WGM of a free-standing micro-bubble, its resonance undergoes a red shift as the temperature increases incrementally. (b) When employing a CTL locking to a typical WGM of a mounted microbubble, the TQP becomes evident when the temperature reaches 25.18 °C.

system could be achieved by employing a more substantial amount of glue to fix two ends of the micro-capillary tube. The inset of Figs. 3(c)–(f) shows the histogram depicting the distribution of the TQP for all WGMs within the specified frequency range for the cases of adding several combined fixed positions. These simple statistical findings once again confirm the conclusions that the temperature at the TQP tends to rise as more fixed positions are added.

As mentioned before, distinct modes exhibit varying slopes in their resonance frequency shifts as the temperature changes. This phenomenon occurs because the pulling force induces strain in the microbubble cavity, causing alterations in the refractive index distribution within its spatial domain. Consequently, the impact on distinct WGM families varies. For instance, the lower order optical modes is positioned around the equator, which is susceptible to the pulling force arising from the thermal expansion of the Al holder. The higher order modes in the microbubble is far away from the equator, characterized by a thicker shell and larger radius, as shown inset in Fig. 4. Figs. 4(a) and (b) shows the typical transmission spectra of the mounted microbubble resonator with different coupling positions (P1 & P2). As the coupling position shifts towards higher latitudes, the overall count of TQPs tends to decrease. Obviously, it is harder to tune the higher order modes through the application of the pulling force arising from the thermal expansion. As the latitude increases, this force has a minimal impact in regions away from the equator. As depicted in Fig. 4(b), the representative resonance indicated by the dashed curve exhibits an approximately linear red shift with temperature. The reason is that the thermo-refractive and thermal-expansion of the microcavity dominates, and the pulling force originating from the thermal expansion of the Al holder exerts minimal influence.

In addition, we have conducted an investigation into the resonance frequency shift with changing temperature and identified the TQP within the fixed microbubble resonator. To precisely measure the frequency shift, the tunable laser is locked to a specific WGM using the Pound-Drever-Hall-locking (PDH-locking) technique [46]. Then, the laser is heterodyned with a highly stable laser (stabi λ laser) using a photodetector, as depicted in Fig. 1(a). We observed the resulting beat signal using a frequency counter to identify any deviations or fluctuations in the resonance frequency. The quality factor of the employed optical modes are around $\sim 10^7$. Fig. 5(a) shows the resonance consistently shifts towards the red side in the free-standing microbubble when the temperature is incrementally increased from 25 °C to 25.2 °C with the slope of 1.25 GHz/°C. While in a proposed fixed micro-bubble, the resonance does not exhibit a linear shift in response to changes in temperature. The TQP becomes apparent once the temperature reaches 25.18 °C, as shown in Fig. 5(b). An athermal microcavity can be achieved at the TQP, which agrees well with the previous results. When the temperature stabilizes at the TQP, the resulting resonance frequency shift is minimal, making it suitable for laser stabilization.

III. Conclusion

In summary, we have demonstrated a method to mitigate the thermal effects in the mounted microbubble resonator. To counteract the resonance red-shift caused by thermo-refractive effects and thermal expansion of the SiO_2, the microbubble resonator's radius is reduced by the pulling force exerted by the Al holder on the capillary tube's pole. This, in turn, induces a blue-shift in the resonance of the microbubble resonator. By ingeniously converting the thermal expansion of the Al holder into a change in the diameter of a microbubble resonator, we have attained an athermal effect at an appropriate temperature. This athermal effect results from the compensation achieved through the diminishing pulling force of thermal expansion counteracting the

effects of thermo-refraction and material expansion. The optical modes located around the equator are particularly susceptible to the influence of this pulling force. These distinctive and insensitive characteristics pave the way for a novel approach to creating temperature-insensitive microresonators using these mounted devices or increasing temperature sensitivity by employing pressed microbubble microresonators.

ACKNOWLEDGMENT

This work was partially carried out at the USTC Center for Micro and Nanoscale Research and Fabrication. The authors thank C.-L. Zou for helpful discussion.

REFERENCES

[1] T. Aoki et al., "Observation of strong coupling between one atom and a monolithic microresonator," *Nature*, vol. 443, no. 7112, Oct. 2006, Art. no. 671.
[2] M. Aspelmeyer, T. J. Kippenberg, and F. Marquardt, "Cavity optomechanics," *Rev. Mod. Phys.*, vol. 86, no. 4, Dec. 2014, Art. no. 1391.
[3] Y. Zhi, X.-C. Yu, Q. Gong, L. Yang, and Y.-F. Xiao, "Single nanoparticle detection using optical microcavities," *Adv. Mater.*, vol. 29, no. 12, Mar. 2017, Art. no. 1604920.
[4] C.-H. Dong, Y.-D. Wang, and H.-L. Wang, "Optomechanical interfaces for hybrid quantum networks," *Nat. Sci. Rev.*, vol. 2, no. 4, Dec. 2015, Art. no. 510.
[5] L. He, S. K. Ozdemir, and L. Yang, "Whispering gallery microcavity lasers," *Laser Photon. Rev.*, vol. 7, no. 1, Jan. 2013, Art. no. 60.
[6] J. Liu et al., "Emerging material platforms for integrated microcavity photonics," *Sci. China: Phys. Mech. Astron.*, vol. 65, no. 10, Oct. 2022, Art. no. 104201.
[7] C. Wang et al., "Soliton formation and spectral translation into visible on CMOS-compatible 4h-silicon-carbide-on-insulator platform," *Light: Sci. Appl.*, vol. 11, no. 1, Dec. 2022, Art. no. 341.
[8] D. Zhu et al., "Spectral control of nonclassical light pulses using an integrated thin-film lithium niobate modulator," *Light: Sci. Appl.*, vol. 11, no. 1, Nov. 2022, Art. no. 327.
[9] J. Guo and S. Groblacher, "Integrated optical-readout of a high-q mechanical out-of-plane mode," *Light: Sci. Appl.*, vol. 11, no. 1, Sep. 2022, Art. no. 282.
[10] Y. Hu et al., "Generation of optical frequency comb via giant optomechanical oscillation," *Phys. Rev. Lett.*, vol. 127, no. 13, Sep. 2021, Art. no. 134301.
[11] Y. Wang et al., "Realization of quantum ground state in an optomechanical crystal cavity," *Sci. China: Phys. Mech. Astron.*, vol. 66, 2023, Art. no. 124213.
[12] W. Mao, Y. Li, X. Jiang, Z. Liu, and L. Yang, "A whispering-gallery scanning microprobe for raman spectroscopy and imaging," *Light: Sci. Appl.*, vol. 12, no. 1, Oct. 2023, Art. no. 247.
[13] K. J. Vahala, "Optical microcavities," *Nature*, vol. 424, no. 6950, Aug. 2003, Art. no. 839.
[14] X. Jiang et al., "Chaos-assisted broadband momentum transformation in optical microresonators," *Science*, vol. 358, no. 6361, Oct. 2017, Art. no. 344.
[15] T. Carmon, L. Yang, and K. J. Vahala, "Dynamical thermal behavior and thermal self-stability of microcavities," *Opt. Exp.*, vol. 12, no. 20, Oct. 2004, Art. no. 4742.
[16] J. R. Stone, T. C. Briles, T. E. Drake, D. T. Spencer, and S. B. Papp, "Thermal and nonlinear dissipative-soliton dynamics in kerr microresonator frequency combs," *Phys. Rev. Lett.*, vol. 121, no. 6, Aug. 2017, Art. no. 063902.
[17] X. Jiang and L. Yang, "Optothermal dynamics in whispering-gallery microresonators," *Light- Sci. Appl.*, vol. 9, no. 1, Feb. 2020, Art. no. 24.
[18] C.-H. Dong et al., "Fabrication of high-Q polydimethylsiloxane optical microspheres for thermal sensing," *Appl. Phys. Lett.*, vol. 94, no. 23, Jun. 2009, Art. no. 231119.
[19] H. Zhou et al., "Soliton bursts and deterministic dissipative kerr soliton generation in auxiliaryassisted microcavities," *Light: Sci. Appl.*, vol. 8, no. 1, May 2019, Art. no. 50.
[20] Z.-D. Peng, C.-Q. Yu, H.-L. Ren, C.-L. Zou, G.-C. Guo, and C.-H. Dong, "Gas identification in high-q microbubble resonators," *Opt. Lett.*, vol. 45, no. 16, Aug. 2020, Art. no. 4440.
[21] L. He, Y.-F. Xiao, J. Zhu, S. K. Ozdemir, and L. Yang, "Oscillatory thermal dynamics in high-Q PDMS-coated silica toroidal microresonators," *Opt. Exp.*, vol. 17, no. 12, Jun. 2009, Art. no. 9571.
[22] Z.-C. Luo, C.-Y. Ma, B.-B. Li, and Y.-F. Xiao, "Mhz-level self-sustained pulsation in polymer microspheres on a chip," *AIP Adv.*, vol. 4, no. 12, Dec. 2014, Art. no. 122902.
[23] Y. Deng, F. Liu, Z. C. Leseman, and M. Hossein-Zadeh, "Thermo-optomechanical oscillator for sensing applications," *Opt. Exp.*, vol. 21, no. 4, Feb. 2013, Art. no. 4653.
[24] Z.-Y. Wang et al., "Thermal oscillation in the hybrid Si_3N_4 - TiO_2 microring," *Opt. Exp.*, vol. 31, no. 3, Jan. 2023, Art. no. 4569.
[25] X. Sun, H. Liang, R. Luo, W. C. Jiang, X.-C. Zhang, and Q. Lin, "Nonlinear optical oscillation dynamics in high-Q lithium niobate microresonators," *Opt. Exp.*, vol. 25, no. 12, Jun. 2017, Art. no. 13504.
[26] Y.-S. Park and H. Wang, "Regenerative pulsation in silica microspheres," *Opt. Lett.*, vol. 32, no. 21, Nov. 2007, Art. no. 3104.
[27] J. Park et al., "Titanium dioxide whispering gallery microcavities," *Adv. Opt. Mater.*, vol. 2, no. 8, Aug. 2014, Art. no. 711.
[28] N. M. Kondratiev and M. L. Gorodetsky, "Thermorefractive noise in whispering gallery mode microresonators: Analytical results and numerical simulation," *Phys. Lett. A*, vol. 382, Aug. 2017, Art. no. 2265.
[29] G. Huang et al., "Thermorefractive noise in silicon-nitride microresonators," *Phys. Rev. A*, vol. 99, no. 6, Jun. 2019, Art. no. 061801.
[30] B. Guha, J. Cardenas, and M. Lipson, "Athermal silicon microring resonators with titanium oxide cladding," *Opt. Exp.*, vol. 21, no. 22, Nov. 2013, Art. no. 26557.
[31] S. S. Djordjevic et al., "CMOS-compatible, athermal silicon ring modulators clad with titanium dioxide," *Opt. Exp.*, vol. 21, no. 12, Jun. 2013, Art. no. 13958.
[32] J. Bovington, S. Srinivasan, and J. E. Bowers, "Athermal laser design," *Opt. Exp.*, vol. 22, no. 16, Aug. 2014, Art. no. 19357.
[33] S. Feng et al., "Athermal silicon ring resonators clad with titanium dioxide for 1.3 m wavelength operation," *Opt. Exp.*, vol. 23, no. 20, Oct. 2015, Art. no. 25653.
[34] F. Qiu, A. M. Spring, and S. Yokoyama, "Athermal and high-q hybrid TiO_2-Si_3N_4 ring resonator via an etchingfree fabrication technique," *ACS Photon.*, vol. 2, no. 3, Mar. 2015, Art. no. 405.
[35] T. J. Wang, P. K. Chen, Y. T. Li, and A. N. Sung, "Athermal high-Q tantalum-pentoxide-based microresonators on silicon substrates," *Opt. Laser Technol.*, vol. 138, Jun. 2021, Art. no. 106925.
[36] Z.-Y. Wang, P.-Y. Wang, M. Li, S. Wan, G.-C. Guo, and C.-H. Dong, "Numerical characterization of soliton microcomb in an athermal hybrid $Si_3N_4CTiO_2$ microring," *Appl. Opt.*, vol. 61, no. 15, May 2022, Art. no. 4329.
[37] C. C. Evans, C. Liu, and J. Suntivich, "Low-loss titanium dioxide waveguides and resonators using a dielectric lift-off fabrication process," *Opt. Exp.*, vol. 23, no. 9, May 2015, Art. no. 11160.
[38] J. Lim et al., "Chasing the thermodynamical noise limit in whisperinggallery-mode resonators for ultrastable laser frequency stabilization," *Nature Commun.*, vol. 8, no. 1, Mar. 2017, Art no. 8.
[39] M. Sumetsky, Y. Dulashko, and R. Windeler, "Super free spectral range tunable optical microbubble resonator," *Opt. Lett.*, vol. 35, no. 11, Jun. 2010, Art. no. 1866.
[40] S. Berneschi et al., "High Q silica microbubble resonators fabricated by arc discharge," *Opt. Lett.*, vol. 36, no. 17, Sep. 2011, Art. no. 3521.
[41] Q. Lu, S. Liu, X. Wu, L. Liu, and L. Xu, "Stimulated brillouin laser and frequency comb generation in high-Q microbubble resonators," *Opt. Lett.*, vol. 41, no. 8, Apr. 2016, Art. no. 1736.
[42] J. Liao, A. Qavi, M. Adolphson, and L. Yang, "High-Q WGM resonators encapsulated in PDMS for highly sensitive displacement detection," *J. Lightw. Technol.*, vol. 41, no. 9, May 2023, Art. no. 2862.
[43] Z. Wang et al., "Monitoring and identifying pendant droplets in microbottle resonators," *Photon. Res.*, vol. 10, no. 3, Mar. 2022, Art. no. 662.
[44] Y. Chen, Z.-H. Zhou, C.-L. Zou, Z. Shen, G.-C. Guo, and C.-H. Dong, "Tunable raman laser in a hollow bottle-like microresonator," *Opt. Exp.*, vol. 25, no. 14, Jul. 2017, Art. no. 16879.
[45] A. Arbabi and L. L. Goddard, "Measurements of the refractive indices and thermo-optic coefficients of Si_3N_4 and siox using microring resonances," *Opt. Lett.*, vol. 38, no. 19, Oct. 2013, Art. no. 3878.
[46] R. Niu et al., "kHz-precision wavemeter based on reconfigurable microsoliton," *Nature Commun.*, vol. 14, no. 1, Jan. 2023, Art. no. 169.